Acta Crystallographica Section D
Biological Crystallography
ISSN 0907-4449

Towards investigation of the inhibitor-recognition mechanisms of drug-target proteins by neutron crystallography

Ryota Kuroki,* Nobuo Okazaki, Motoyasu Adachi, Takashi Ohhara, Kazuo Kurihara and Taro Tamada

Molecular Biology Research Center, Quantum Beam Science Directorate, Japan Atomic Energy Agency, 2-4 Shirakata-shirane, Tokai, Ibaraki 319-1195, Japan

Correspondence e-mail: kuroki.ryota@jaea.go.jp

Received 15 April 2010
Accepted 30 August 2010

It is generally known that enzymes represent important drug-target proteins. Elucidation of the catalytic function and the molecular-recognition mechanisms of enzymes provides important information for structure-based drug design. Neutron crystallography provides accurate information on the locations of H atoms that are essential in enzymatic function and molecular recognition. Recent examples are described of the structure determination of the drug-target proteins human immunodeficiency virus protease and porcine pancreatic elastase in complex with transition-state analogue inhibitors using the neutron diffractometers for biological crystallography (BIX-3 and BIX-4) installed at the JRR-3 research reactor.

1. Introduction

Increasing the number of solved protein structures will enable us to understand protein function as well as to create useful molecules. X-ray crystallography is the most popular technique for obtaining protein structure information. It is known that H atoms play crucial roles in the molecular recognition and catalytic reactions of enzymes. The locations of H atoms in protein molecules are usually predicted by theoretical approaches, but it is still very difficult to determine the ionization status of catalytic residues, the hydration structure and the characteristics of hydrogen-bonding interactions, especially low-barrier hydrogen-bonding interactions. There are two approaches to observing the location of H atoms: ultrahigh-resolution X-ray crystallography and neutron crystallography (Myles, 2006; Niimura & Bau, 2008). Since X-ray diffraction shows the location of the electron, the bond distance is sometimes different when observed by neutron diffraction. On the basis of these features, we attempted to determine protein structures using both X-ray and neutron diffraction. Three different data sets were collected, including X-ray diffraction data at 100 K and room-temperature and neutron diffraction data at room temperature (using exactly the same crystal as used for X-ray data collection at room temperature). Here, we report successful examples of the structure determination of human immunodeficiency virus (HIV-1) protease and porcine pancreatic elastase (PPE) using a combination of neutron and X-ray diffraction data.

More than 60 000 X-ray structures have been archived in the Protein Data Bank; although neutron crystallography is a powerful tool for determining the locations of H atoms, neutron diffraction has contributed a total of at most 40 structures (http://www.pdb.org/). Therefore, further technical developments are needed for further effective utilization of neutron diffraction in protein structure determination. Our

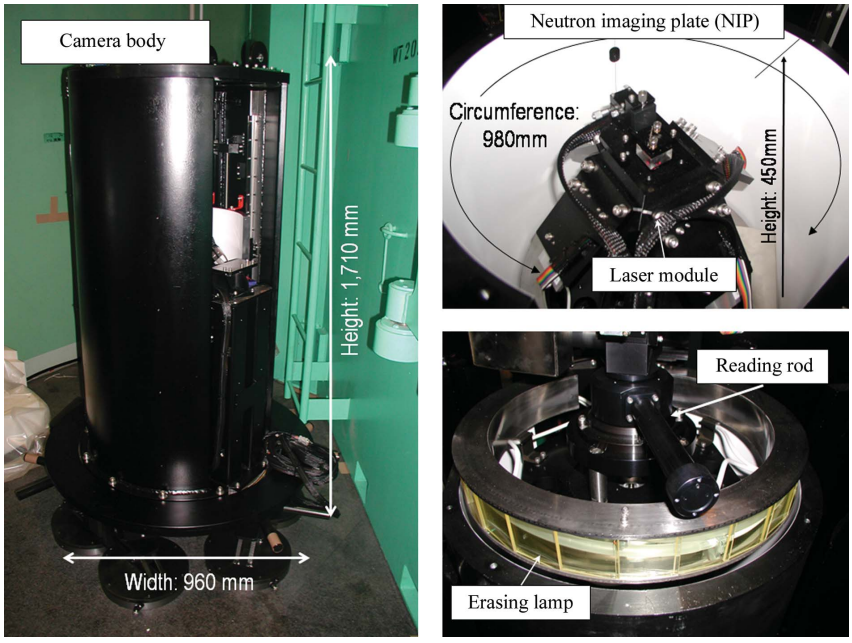

Figure 1
The BIX-4 neutron diffractometer at JRR-3. The camera body of BIX-4 is shown (left) and its main components: the NIP and laser modules (top right) and the reading rod and erasing lamp (bottom right). The camera body (height = 1710 mm, width = 960 mm) is covered by a cylindrical shielding (not shown) composed of two layers: a 50 mm thick B4C+ resin shield against neutrons and a 50 mm thick lead shield against γ rays.

approaches to developing crystallization and changing the crystal lattice by protein engineering are also described.

2. Neutron structure analysis of drug-target enzymes

2.1. Neutron diffractometers

Neutron diffractometers (BIX-3 and BIX-4) equipped with neutron imaging plates (NIPs) were designed and built by Niimura and coworkers (Tanaka *et al.*, 2002; Kurihara *et al.*, 2004). These diffractometers are installed at the 1G-A and 1G-B ports, respectively, of the JRR-3 research reactor at Japan Atomic Energy Agency, Tokai, Japan. The basic architectures of BIX-3 and BIX-4 are essentially the same. In Fig. 1, the appearance of the camera body of BIX-4 is shown. The NIP covers a large solid angle subtended at the sample with a fine positional linearity, a high spatial accuracy and good neutron detector efficiency. The circumference of the NIP cylinder is 980 mm ($2\theta_S$ angle range = $\pm 140^\circ$),

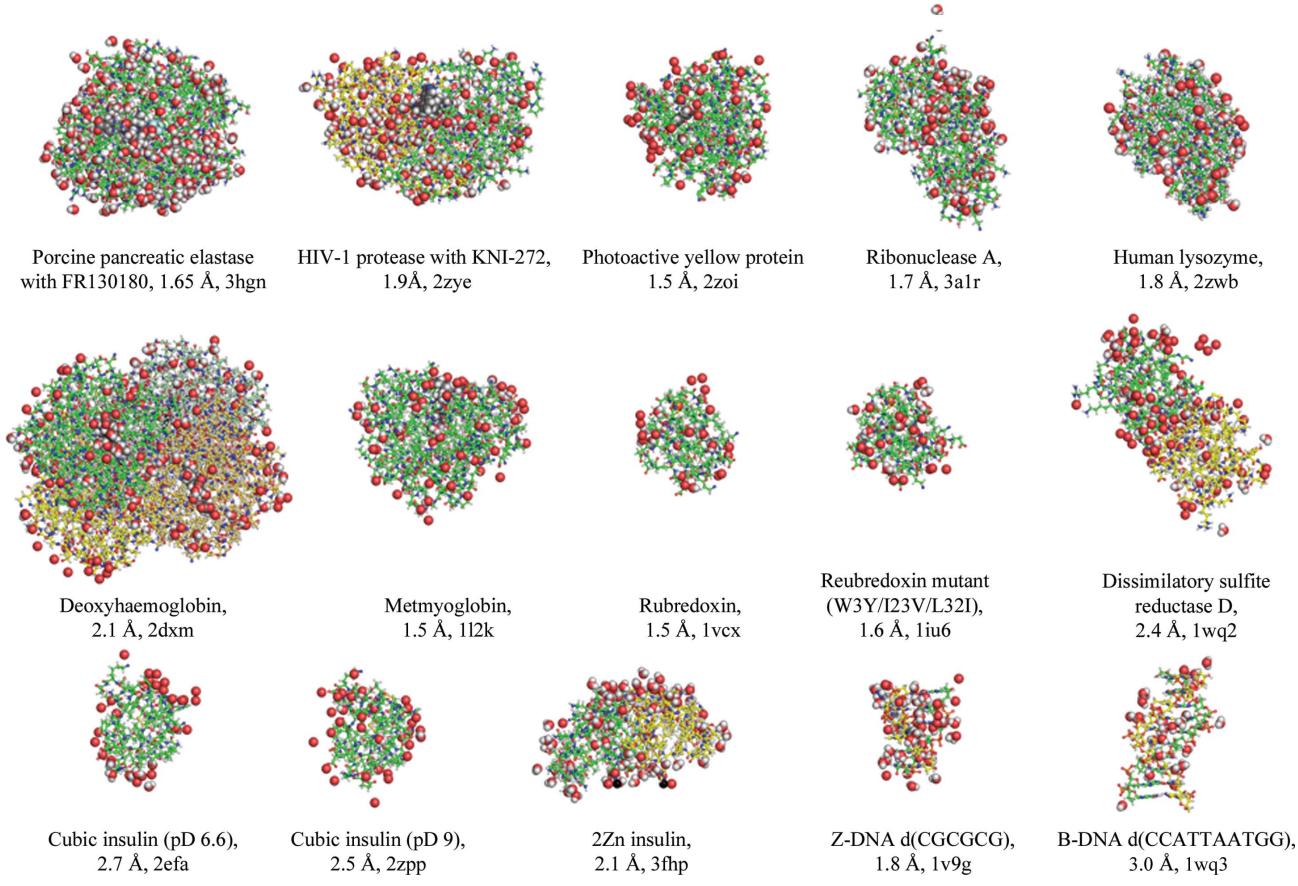

Figure 2
Tertiary structures of biological macromolecules obtained using BIX-3 and BIX-4. A total of 15 structures of biological macromolecules have been determined using BIX-3 and BIX-4 since 2002 and are shown as space-filling representations. The molecular name, resolution and PDB code of each sample are shown under the structure models. Figs. 2, 3 and 4 were drawn using the program *PyMOL* (http://pymol.org/).

its height is 450 mm and the camera radius is 200 mm. The wavelengths of the incident neutrons for BIX-3 and BIX-4 are 2.9 and 2.6 Å, respectively. According to these wavelength values the d_{min} values along the equator line, *i.e.* the highest possible resolution values, are 1.53 and 1.38 Å, respectively. Since 2002 BIX-3 and BIX-4 have contributed to 15 structure determinations of biological macromolecules (as shown in Fig. 2).

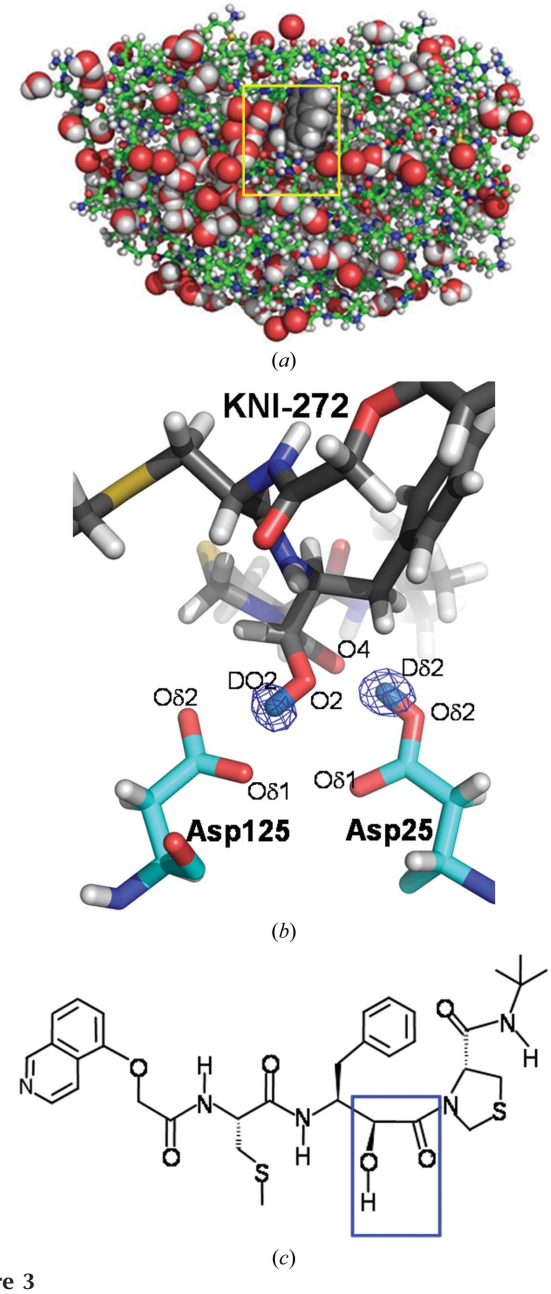

Figure 3
Tertiary structure of HIV-1 protease in complex with its inhibitor determined by neutron diffraction. (*a*) Overall dimer structure of HIV-1 protease determined by neutron diffraction. The HIV-1 protease is shown as a ball-and-stick model; water molecules and bound inhibitor are shown in space-filling representation. H and D, C, O, N and S atoms are represented in white, cyan, red, blue and yellow, respectively. C atoms in KNI-272 are shown in dark grey. (*b*) Interaction between the active site and KNI-272 in the yellow box in (*a*). The $|F_o - F_c|$ OMIT nuclear density map shown at the 5σ level in blue was calculated without the contributions of the Dδ2 and DO2 atoms. (*c*) Chemical structure of the inhibitor KNI-272. The blue box indicates the hydroxymethylcarbonyl moiety.

2.2. Data collection and refinement

Neutron diffraction data collections using BIX-3 and BIX-4 were usually carried out at room temperature with protein

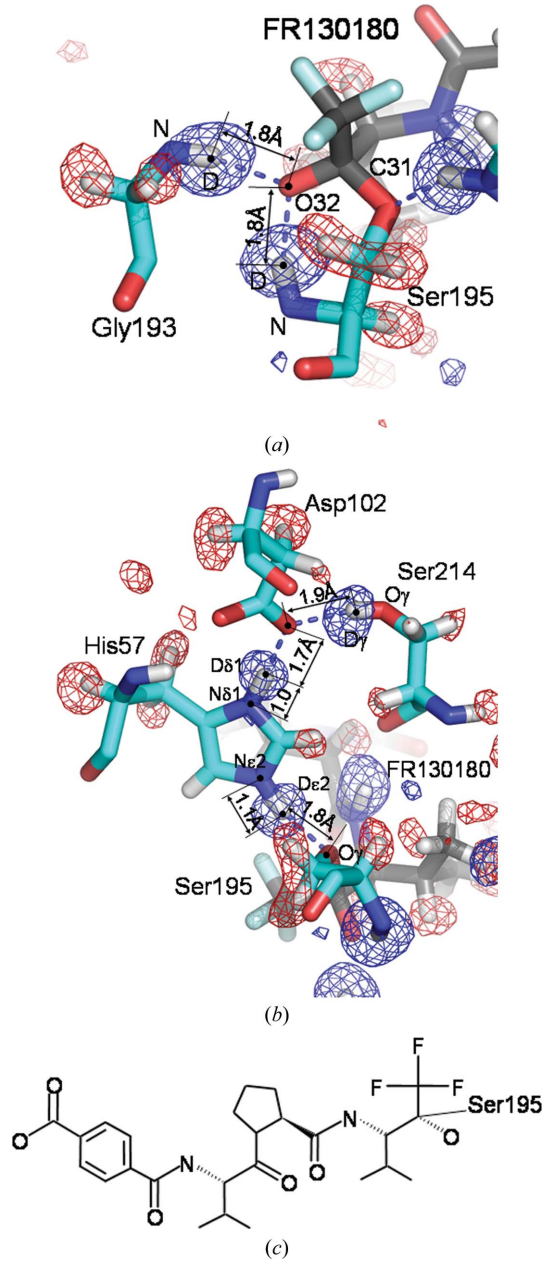

Figure 4
Inhibitor recognition of PPE determined by neutron diffraction. (*a*) Tertiary structure of the oxyanion hole of PPE. H and D, C, O and N atoms are represented in white, cyan, red and blue, respectively. C atoms in FR130180 are shown in dark grey. The $|F_o - F_c|$ OMIT nuclear density maps were calculated without the contributions of H and D atoms. The blue and red contours show +5.0σ and −4.5σ densities, respectively. (*b*) Tertiary structure of the catalytic triad of PPE. The $|F_o - F_c|$ nuclear density maps were calculated as above. (*c*) Chemical structure of FR130180.

crystals of 1–10 mm^3 in volume. The intensity data were processed using the programs *DENZO* and *SCALEPACK* (Otwinowski & Minor, 1997). After neutron data collection, the same crystals were used to collect X-ray diffraction data for joint neutron/X-ray refinement (Wlodawer & Hendrickson, 1982; Adams *et al.*, 2009). The diffraction data were processed using *HKL*-2000 (Otwinowski & Minor, 1997).

Coordinate sets for neutron structures were obtained using the joint refinement method with the program *PHENIX* (Adams *et al.*, 2010), which used 1.9 Å neutron and 1.4 Å X-ray diffraction data sets for HIV-1 protease (Adachi *et al.*, 2009) and 1.65 Å neutron and 1.2 Å X-ray diffraction data sets for PPE (Tamada *et al.*, 2009). Manual model modifications in these refinements were carried out using the programs *XtalView* (McRee, 1992), *Coot* (Emsley & Cowtan, 2004) and *QUANTA* (Accelrys Inc., San Diego, California, USA).

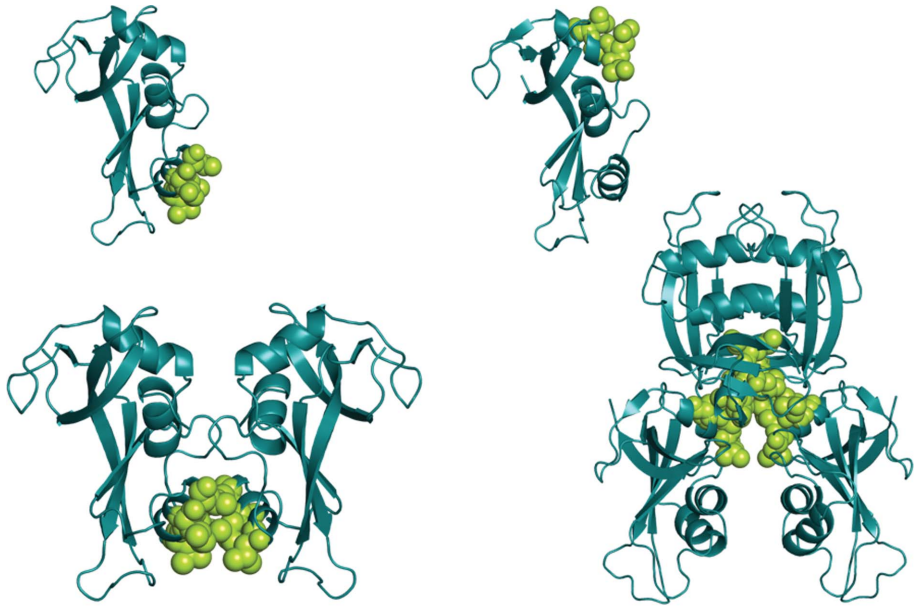

Figure 5
Leucine-induced artificial association of mutant human RNase-1. (*a*) Association of the 4L mutant human RNase 1 in which four leucines were incorporated into helix 2. Two mutant RNases were associated by leucines (shown as van der Waals representations). (*b*) Association of the N4L mutant human RNase 1 in which four leucines were incorporated into helix 3. Four mutant RNases were associated; the incorporated leucines are shown as van der Waals representations.

High-resolution X-ray diffraction data were also collected from a crystal with a volume of ∼0.001 mm^3 at 100 K at the synchrotron-radiation sources SPring-8 (Hyogo, Japan) and Photon Factory (Tsukuba, Japan) and were processed using *HKL*-2000. High-resolution X-ray structures for each protein were refined using *CNS* (Brünger *et al.*, 1998) followed by *SHELX*-97 (Sheldrick, 2008).

2.3. Structure of HIV-1 protease in complex with the potent inhibitor KNI272

HIV-1 protease is a dimeric aspartic protease that contains two aspartic acid residues as catalytic residues (defined as residue positions Asp25 and Asp125) and plays an essential role in viral replication. To develop HIV-1 protease inhibitors through structure-based drug design, it is useful to understand the catalytic mechanism and inhibitor recognition of HIV-1 protease. Thus, we determined all atom positions, including H atoms, of HIV-1 protease in complex with KNI-272 using neutron diffraction (PDB code 2zye; Adachi *et al.*, 2009; Figs. 3*a* and 3*b*). The inhibitor KNI-272 used in this study contains a hydroxymethylcarbonyl isostere moiety (shown in a blue box in Fig. 3*c*) that interacts with the catalytic residues of HIV-1 protease. The neutron diffraction analysis directly showed that Asp25 is protonated and that Asp125 is unprotonated (Fig. 3*b*). Although the catalytic mechanism of HIV-1 protease has been a matter of some debate, our results demonstrate that Asp25 provides a proton to the carbonyl group of the substrate and Asp125 contributes to activating the attacking water molecule as a nucleophile. The structural information, including the protonation states of the catalytic residues, determined in this study will provide us with important information for the design of more effective inhibitors.

2.4. Structure of porcine pancreatic elastase in complex with the potent inhibitor FR130180

Elastase is a serine protease classified in the chymotrypsin family and is possibly the most destructive enzyme, with an ability to degrade virtually all of the connective components in the body. To help resolve long-standing questions regarding the catalytic activity of the serine proteases, the structure of PPE has been analyzed by combined high-resolution neutron and X-ray crystallography (Figs. 4*a* and 4*b*). In this analysis, the peptidic inhibitor FR130180 (chemical structure shown in Fig. 4*c*) was used to mimic the tetrahedral intermediate. A single large crystal for diffraction experiments was prepared by repeating macroseeding into a crystallization solution prepared with deuterated reagents (Kinoshita *et al.*, 2007).

The tertiary structure of PPE in complex with FR130180 was determined to 1.65 Å resolution by neutron crystallography and also to 1.20 Å resolution by X-ray crystallography using diffraction data obtained at room temperature from the same crystal (PDB code 3hgn; Tamada *et al.*, 2009). The complex structure includes a total of 1792 H and D atoms and 190 hydration water molecules. The neutron analysis showed that the O atom of the oxopropyl group of the inhibitor was present as an oxygen anion rather than a hydroxyl group (Fig. 4*a*) because the O atom (O32) was directed towards the D (H) atoms of the backbone amides of Gly193 and Ser195 and no nuclear density was observed for deuterium attached to O32.

The neutron and X-ray data also show that the hydrogen bond between His57 and Asp102 (chymotrypsin numbering) is 2.6 Å in length and that the hydrogen-bonding hydrogen is 0.8–1.0 Å from the histidine N atom (Fig. 4*b*). This is not consistent with a low-barrier hydrogen bond, which would be predicted to position the hydrogen midway between the donor and acceptor atoms. The observed interaction between His57 and Asp102 is essentially a short but conventional hydrogen bond, sometimes described as a short ionic hydrogen bond.

3. Future aspects of solving the problem of enzyme–inhibitor interaction by neutron crystallography

It is generally known that a large-volume crystal (1.0–10 mm^3) is needed for neutron diffraction because of the weak diffraction. Since reducing the unit-cell volume of a protein crystal empirically improves the maximum diffraction resolution by strengthening the diffraction intensities, engineering of the protein crystal lattice to change the space group should contribute to reducing the neutron data-collection time by improving the symmetry. We have attempted 'crystal lattice engineering' to change the packing and the space group by introducing a new interface. The first attempts involved the incorporation of a leucine zipper-like hydrophobic interface (comprising four leucine residues) into a helical region (helix 2) of human pancreatic ribonuclease 1 (RNase 1). The mutant RNase 1 was successfully crystallized in space group $I4_1$, with a unit-cell volume of 412 678.7 $Å^3$, and the crystal structure was subsequently determined by X-ray crystallography (Yamada *et al.*, 2007). The overall structure of 4L-RNase 1, in which amino acids at four positions were mutated to leucine, is quite similar to that of bovine RNase A and the introduced leucine residues formed the designed crystal interface (Fig. 5*a*). To further characterize the role of the introduced leucine residues in the crystallization of RNase 1, the number of leucines was reduced to three or two (3L-RNase 1 and 2L-RNase 1, respectively). Both mutants crystallized and a similar hydrophobic interface to that in 4L-RNase 1 was observed.

A related approach of engineering crystal contacts at helix 3 of RNase 1 (N4L-RNase 1) was also evaluated. N4L-RNase 1 was also successfully crystallized in space group $P6_122$, with a unit-cell volume of 941 059.7 $Å^3$, and formed the expected hydrophobic packing interface. In Fig. 5(*b*), the crystal packings of 4L-RNase 1 and N4L-RNase 1 are shown. These results suggest that the appropriate introduction of a unique leucine zipper-like hydrophobic interface can promote intermolecular symmetry, *i.e.* twofold for more efficient protein crystallization in crystal lattice engineering efforts, and may optimize the crystal lattice for neutron crystallography.

We thank the beamline staffs at SPring-8 (proposal Nos. 2005B0982 and 2007A1513) and the Photon Factory (proposal Nos. 2007G212 and 2008G075). We are also indebted to the members of the SOSHO project at Osaka University, especially Professors H. Matsumura, H. Adachi and Y. Mori, and Professors T. Kinoshita and T. Tada of Osaka Prefecture University for the crystallization of HIV-1 protease and porcine pancreatic elastase, respectively. We also thank Professor M. Blaber of Florida State University for reading the manuscript. This work was supported in part by MEXT Grants-in-Aid for Scientific Research (B) (19370046 and 22390010) to RK.

References

Adachi, M. *et al.* (2009). *Proc. Natl Acad. Sci. USA*, **106**, 4641–4646.
Adams, P. D. *et al.* (2010). *Acta Cryst.* D**66**, 213–221.
Adams, P. D., Mustyakimov, M., Afonine, P. V. & Langan, P. (2009). *Acta Cryst.* D**65**, 567–573.
Brünger, A. T., Adams, P. D., Clore, G. M., DeLano, W. L., Gros, P., Grosse-Kunstleve, R. W., Jiang, J.-S., Kuszewski, J., Nilges, M., Pannu, N. S., Read, R. J., Rice, L. M., Simonson, T. & Warren, G. L. (1998). *Acta Cryst.* D**54**, 905–921.
Emsley, P. & Cowtan, K. (2004). *Acta Cryst.* D**60**, 2126–2132.
Kinoshita, T., Tamada, T., Imai, K., Kurihara, K., Ohhara, T., Tada, T. & Kuroki, R. (2007). *Acta Cryst.* F**63**, 315–317.
Kurihara, K., Tanaka, I., Refai Muslih, M., Ostermann, A. & Niimura, N. (2004). *J. Synchrotron Rad.* **11**, 68–71.
McRee, D. E. (1992). *J. Mol. Graph.* **10**, 44–46.
Myles, D. A. (2006). *Curr. Opin. Struct. Biol.* **16**, 630–637.
Niimura, N. & Bau, R. (2008). *Acta Cryst.* A**64**, 12–22.
Otwinowski, Z. & Minor, W. (1997). *Methods Enzymol.* **276**, 307–326.
Sheldrick, G. M. (2008). *Acta Cryst.* A**64**, 112–122.
Tamada, T., Kinoshita, T., Kurihara, K., Adachi, M., Ohhara, T., Imai, K., Kuroki, R. & Tada, T. (2009). *J. Am. Chem. Soc.* **131**, 11033–11040.
Tanaka, I., Kurihara, K., Chatake, T. & Niimura, N. (2002). *J. Appl. Cryst.* **35**, 34–40.
Wlodawer, A. & Hendrickson, W. A. (1982). *Acta Cryst.* A**38**, 239–247.
Yamada, H. *et al.* (2007). *Protein Sci.* **16**, 1389–1397.